New land-use-change emissions indicate a declining CO2 airborne fraction

van Marle, Margreet J.E.; van Wees, Dave; Houghton, Richard A.; Field, Robert D.; Verbesselt, Jan; van der Werf, Guido R.

published in
Nature
2022

DOI (link to publisher)
10.1038/s41586-021-04376-4

document version
Publisher's PDF, also known as Version of record

Article

New land-use-change emissions indicate a declining CO_2 airborne fraction

https://doi.org/10.1038/s41586-021-04376-4

Received: 26 April 2021

Accepted: 20 December 2021

Published online: 16 March 2022

Check for updates

Margreet J. E. van Marle[1,2,7], Dave van Wees[1,7], Richard A. Houghton[3], Robert D. Field[4,5], Jan Verbesselt[6] & Guido. R. van der Werf[1]✉

About half of the anthropogenic CO_2 emissions remain in the atmosphere and half are taken up by the land and ocean[1]. If the carbon uptake by land and ocean sinks becomes less efficient, for example, owing to warming oceans[2] or thawing permafrost[3], a larger fraction of anthropogenic emissions will remain in the atmosphere, accelerating climate change. Changes in the efficiency of the carbon sinks can be estimated indirectly by analysing trends in the airborne fraction, that is, the ratio between the atmospheric growth rate and anthropogenic emissions of CO_2 (refs. [4–10]). However, current studies yield conflicting results about trends in the airborne fraction, with emissions related to land use and land cover change (LULCC) contributing the largest source of uncertainty[7,11,12]. Here we construct a LULCC emissions dataset using visibility data in key deforestation zones. These visibility observations are a proxy for fire emissions[13,14], which are – in turn – related to LULCC[15,16]. Although indirect, this provides a long-term consistent dataset of LULCC emissions, showing that tropical deforestation emissions increased substantially (0.16 Pg C decade^{-1}) since the start of CO_2 concentration measurements in 1958. So far, these emissions were thought to be relatively stable, leading to an increasing airborne fraction[4,5]. Our results, however, indicate that the CO_2 airborne fraction has decreased by 0.014 ± 0.010 decade^{-1} since 1959. This suggests that the combined land–ocean sink has been able to grow at least as fast as anthropogenic emissions.

Carbon–climate feedbacks constitute a key uncertainty in predicting future climate change[17,18]. Over the past decades, the functioning of carbon sinks has therefore undergone increased scrutiny from the scientific community. However, partly owing to large spatio-temporal variability, direct estimates of the sink strength, its annual variability and trends remain uncertain[11]. Analysing trends in the airborne fraction (AF) provides an independent estimate of the functioning of all sinks combined. Several studies observed an increase in AF[4,5] in line with findings of a decline in CO_2 uptake efficiencies of parts of the land[19–21] and ocean sinks[2,22]. Other studies suggested that the trend is too small to be statistically significant[6], warned against misinterpreting the trend in AF[7] or argued that multiple trends are needed to describe the AF pattern over the past 60 years (refs. [8,9]). These conflicting results highlight the underlying uncertainties in this approach, partly related to uncertainties in datasets used, in particular, those of LULCC emissions.

The uncertainty in the magnitude of LULCC emissions stems, for a large part, from uncertainties in tropical forest losses, especially before satellite observations became available. Although these and other fluxes related to LULCC emissions are nowadays only about 10–20% of fossil fuel emissions, their uncertainty is larger, even in absolute terms[11]. The uncertainty in LULCC emissions has an especially large contribution to the overall uncertainty in anthropogenic emissions during the mid-twentieth century, when LULCC and fossil fuel emissions were more similar in magnitude than they are now.

One avenue that is not exploited in the context of better constraining LULCC emissions is the close link between fire and deforestation[15,16,23]. Fire is the cheapest tool to convert forest to other land uses. In moist tropical rainforests, fires thus signal human presence and deforestation[24]. Even though not all LULCC emissions are associated with fire – logging is a prime example – a better handle on trends in fire emissions in key LULCC regions could provide independent information on temporal dynamics of LULCC emissions.

The two regions with the largest LULCC emissions are South America and Southeast Asia. Fires are routinely measured from satellite, but the longest continuous burned-area dataset starts in 1982 (ref. [25]) and the global emissions record only in 1997 (ref. [26]). However, fires influence visibility and visibility records go back further in time. In this study, we take advantage of the reasonable to good correspondence between fire and visibility in key deforestation regions for the overlapping period[13,14] and use this to convert the visibility record to fire emissions. This allows for the first consistent estimate of fire and related LULCC emissions for the period when direct CO_2 measurements also became available. We use visibility observations as a proxy for fire in the Arc of Deforestation (ARCD), including Brazil and Bolivia, and for Equatorial Asia (EQAS), where most emissions originate from Indonesia, to create a

[1]Department of Earth Sciences, Faculty of Science, Vrije Universiteit Amsterdam, Amsterdam, The Netherlands. [2]Deltares, Delft, The Netherlands. [3]Woodwell Climate Research Center, Falmouth, MA, USA. [4]Department of Physics and Applied Mathematics, Columbia University, New York, NY, USA. [5]NASA Goddard Institute for Space Studies, New York, NY, USA. [6]Laboratory of Geo-information Science and Remote Sensing, Wageningen University, Wageningen, The Netherlands. [7]These authors contributed equally: Margreet J. E. van Marle, Dave van Wees. ✉e-mail: guido.vander.werf@vu.nl

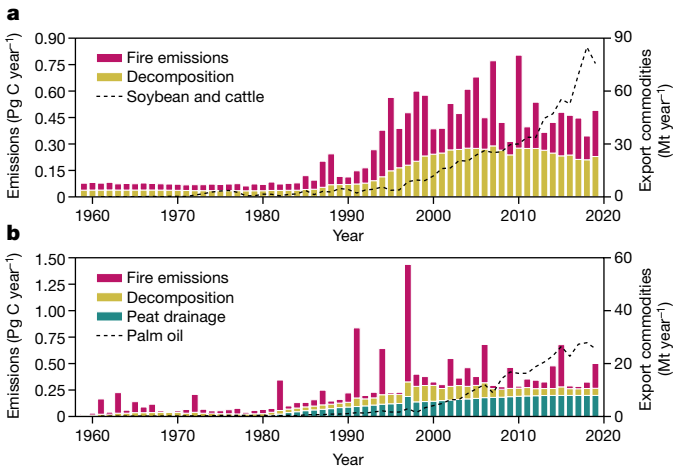

Fig. 1 | Visibility-derived LULCC emissions for two key deforestation regions. Emissions over the period 1959–2019 are shown for ARCD (**a**) and EQAS (**b**). Fire emissions are directly derived from visibility measurements, tuned to match satellite-derived estimates for the overlapping period (1997–2015). These and other emission pathways are described in Methods. Dashed lines depict time series of key commodities derived from deforested areas on the basis of FAOSTAT[44].

consistent estimate of LULCC emissions from these regions since 1958. The two regions account, on average, for 60% of net LULCC emissions over 1959–2019 (ref. [27]). For the other regions, covering the remaining 40%, we relied on improved bookkeeping estimates[27]. Non-fire LULCC emissions were computed on the basis of ancillary data or as a fraction of fire emissions (see Methods).

Our observation-based estimates suggest that fire emissions were relatively low until the early 1980s for EQAS and the late 1980s for the ARCD, after which they increased (Fig. 1). In EQAS, this change reflects more muted fire episodes in Sumatra in the 1960s and 1970s, the absence of severe fire episodes in Borneo until the 1980s and an increase in severity of fire episodes in the 1990s in both regions owing to three strong drought years and intensified deforestation. In the ARCD, it reflects the transition of smallholder to industrial-scale deforestation in the 1980s with an increase in large-scale agriculture[28]. Earlier LULCC estimates also report fire emissions but at a much higher level, especially in the early part of our study period.

Our resulting total LULCC emissions show an increasing trend that resembles the fire reconstruction but at an elevated level owing to the inclusion of other processes and regions (Figs. 1 and 2a). By contrast, LULCC estimates that were used in previous studies assessing the AF had emissions already substantially elevated in the 1960s[29], despite much lower population densities, restricted access to machinery that nowadays facilitates industrial-scale deforestation and the absence of international trade of commodities related to deforested land (Figs. 1 and 2b). More recent versions of the Houghton and Nassikas (2017)[27] dataset (from here on referred to as H&N) support our findings (Fig. 2). Differences with earlier versions as used previously in the Global Carbon Project (from here on referred to as GCP) stem from revised historical data for Latin America, Europe and China, resulting in lower net emissions over 1950–2000 in these regions.

On the basis of our approach, LULCC emissions were, on average, 0.88 Pg C year^{-1} over 1959–2019, slightly lower than H&N (1.04 Pg C year^{-1}, Fig. 2b). By contrast, GCP estimates were 1.41 Pg C year^{-1}, mostly because of higher emission rates between 1960 and 1990 (Fig. 2b). Furthermore, as a result of visibility-based estimates, our dataset shows larger interannual variability than the other two datasets, which may help explain some of the substantial interannual variability in the CO_2 growth rate[30].

We used our new LULCC emission datasets to calculate linear trends in the AF, to identify changes in the strength of the combined land–ocean CO_2 sink. Besides our LULCC emission estimates, we used the average of CO_2 concentrations measured at the Mauna Loa (MLO) and South Pole Observatory (SPO) stations[31] and annual estimates of fossil fuel and cement production emissions[32]. We calculated the trend for: (1) the raw data ('raw'), (2) smoothed data including filtering for the effects of the El Niño–Southern Oscillation (ENSO) and volcanic activity ('filter') and (3) a bootstrapping approach ('bootstrap') (see Methods). In this study, we focused on a single long-term trend, following Raupach et al. (2014)[5].

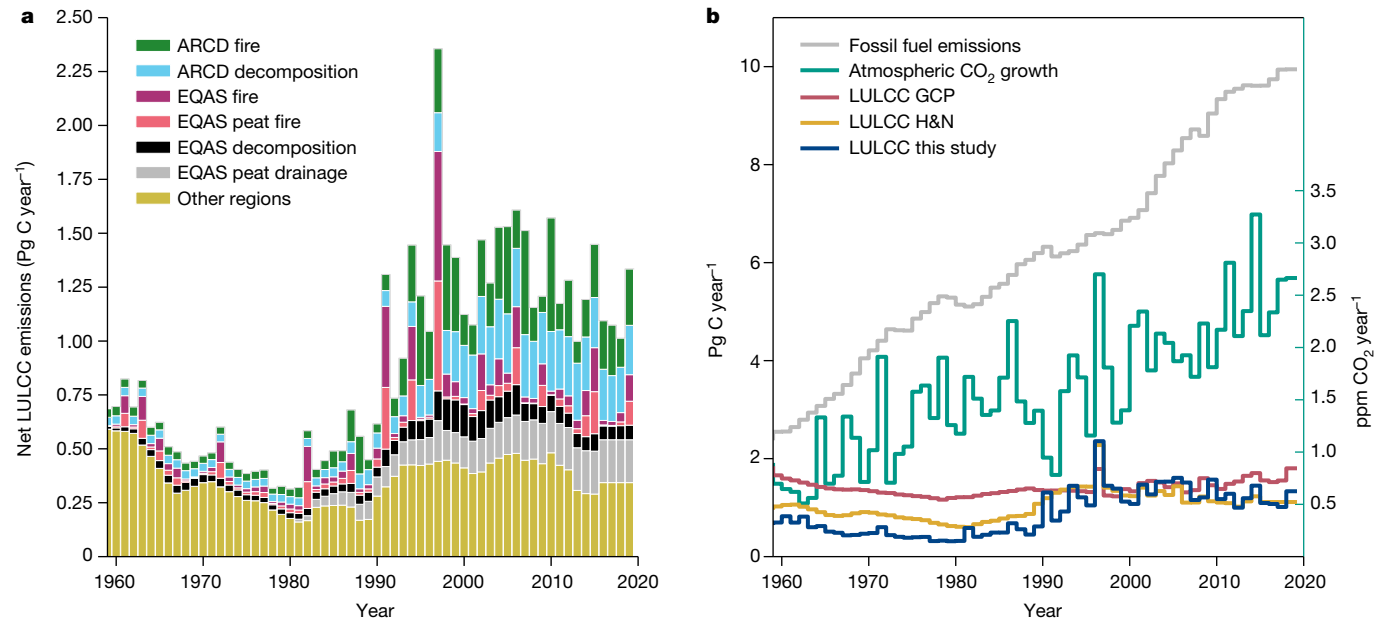

Fig. 2 | Global LULCC emissions and other time series required for computing the AF. a, Global LULCC emissions over the period 1959–2019 from various sources for the Arc of Deforestation (ARCD), Equatorial Asia (EQAS) and other regions. **b**, Global fossil fuel emissions, the atmospheric CO_2 growth rate and LULCC emissions from three datasets, namely, the Global Carbon Project (GCP), Houghton and Nassikas (2017) (H&N) and this study.

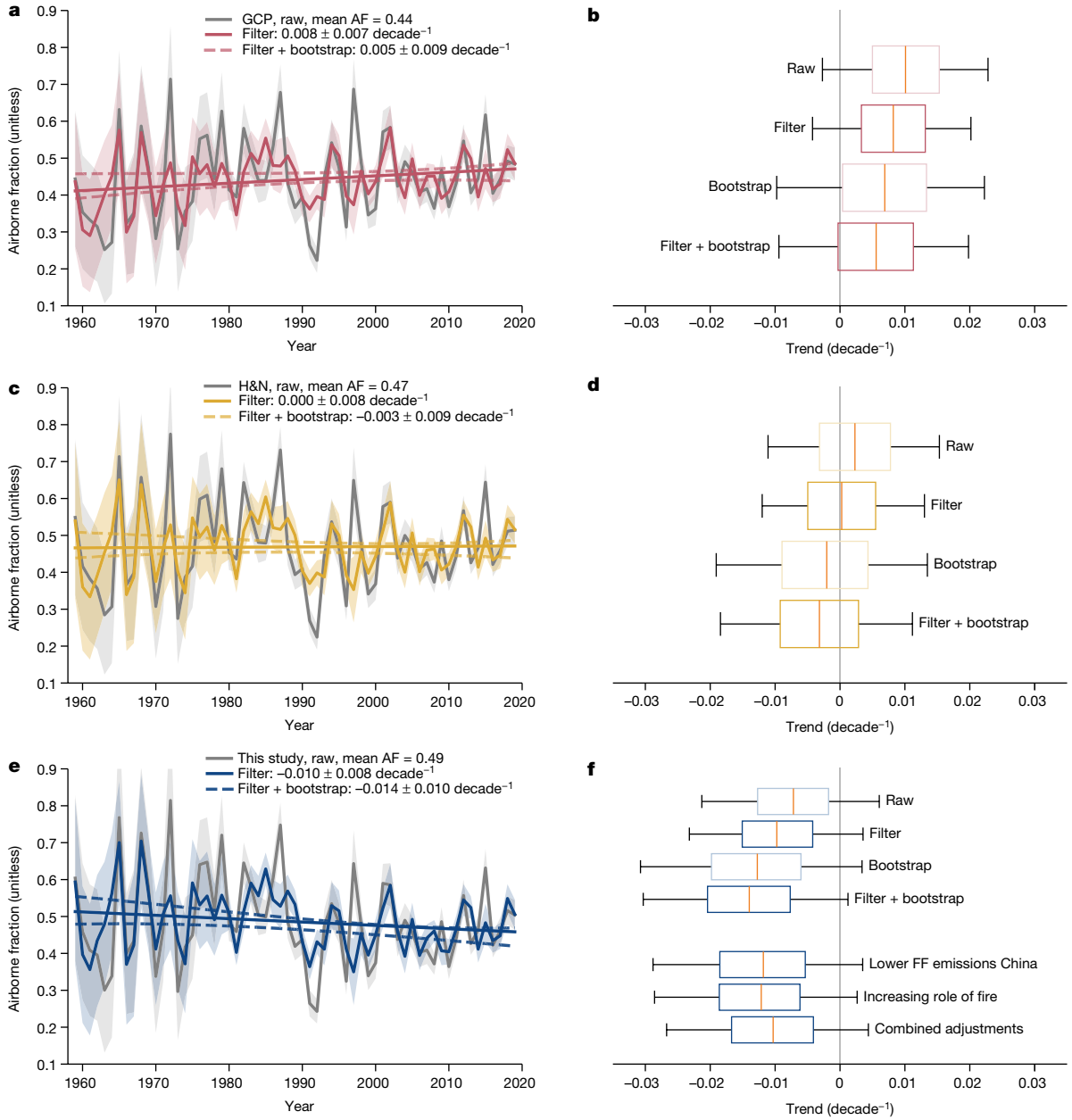

Fig. 3 | AF trend estimates on the basis of three different LULCC emission datasets. LULCC emissions are from the Global Carbon Project (GCP) (**a**, **b**), Houghton and Nassikas (H&N) (**c**, **d**) and this study (**e**, **f**). Left panels, the raw and filtered annual AF time series, with the transparent bands showing the 1σ uncertainty range on the AF trend estimate. Solid trend lines show the mean trend in the filtered AF time series on the basis of a non-parametric Mann–Kendall test and the dashed lines show the 1σ trend uncertainty after uncertainty propagation and bootstrapping (see Methods). The legends show the trend estimates for the raw, filtered and filter + bootstrap data treatments. Right panels, box plots (whiskers are 5% and 95% percentiles) of trend estimates for the raw, filtered, bootstrapped and filter + bootstrap data treatments. For our LULCC estimates, these are supplemented with trend estimates for three adjusted emission scenarios to test the sensitivity of our trend (see Methods). All shown trends and probabilities are on the basis of Monte Carlo simulation with n = 10,000 (see Methods). FF, fossil fuel.

On the basis of our LULCC estimates, the best AF trend estimate ('filter + bootstrap') was −0.014 ± 0.010 decade^{-1} (P = 0.93, probability of negative trend) (Fig. 3 and Table 1). Using the H&N estimates led to a minor negative AF trend (−0.003 ± 0.009 decade^{-1}). For the GCP dataset, we found a positive AF trend of +0.005 ± 0.009 decade^{-1} (P = 0.74, probability of positive trend), in line with most earlier studies that concluded that the combined land–ocean sink had become less efficient over time, implying a reduction in the capacity to take up anthropogenic CO_2 emissions[4,5]. By contrast, the negative AF trend that results from our emission estimates may imply that the combined land–ocean sink has become more efficient over time. The key difference originates from the downward revision of the LULCC emissions in the first half of our study period, leading to higher AF estimates for that period and an overall downward slope (Fig. 3). High probabilities of trend direction (P, probability of positive or negative trend) did not necessarily mean significant trend values owing to large interannual variability in the AF time series (Table 1, columns three and four). However, all of the significant trends (p < 0.05) from a Monte Carlo simulation on the basis of our LULCC estimates were negative (Table 1, columns five and six).

The 1959–2019 average AF was 0.44, 0.47 and 0.49 when using GCP, H&N and our LULCC emissions, respectively (Fig. 3). The declining trend in AF when using our LULCC data constitutes a change in average AF

Table 1 | Airborne fraction trend probabilities

LULCC dataset	Positive	Negative	Positive ($p<0.05$)	Negative ($p<0.05$)	$p<0.05$ (fraction positive)	$p<0.05$ (fraction negative)
GCP	0.74	0.26	0.07	0.00	0.95	0.05
H&N	0.36	0.64	0	0.03	0.09	0.91
This study	0.07	0.93	0	0.25	0	1.00

Trend probabilities were calculated for the three different land use and land cover change (LULCC) emission datasets analysed, namely, the Global Carbon Project (GCP), Houghton and Nassikas (H&N) and this study, on the basis of a Monte Carlo simulation with n=10,000 following the filter + bootstrap data treatment. The first two columns give the fraction of Monte Carlo iterations that resulted in a positive or negative trend. The middle two columns indicate what fraction of these trends was significant at the $p<0.05$ confidence level. The last two columns give the fraction of significant trends that was positive or negative.

from 0.50 during the first decade (1959–1968) to 0.48 during the most recent decade (2010–2019). Given that LULCC estimates carry large uncertainty, we have assessed the sensitivity of the derived trend to changes in the absolute LULCC emissions and their trend (Fig. 4). An upward revision of LULCC emissions (for instance, owing to missing small fires[33]) would, in principle, increase the trend. However, if our temporal evolution of LULCC emissions is right, the LULCC emissions slope increases alongside to this, which – in turn – decreases the AF slope (Fig. 4). Our analysis shows that the latter effect is dominant and, as a result, the AF trend is mostly sensitive to the relative difference between LULCC emissions in the early and the late part of the study period. This provides further support for the robustness of the trend; each step in our estimation of the LULCC emissions is uncertain and there are very little validation data, but the overall increase in fire emissions in deforestation zones over the study period is robust and is supported by proxies such as the increase in trade of deforestation-derived commodities (Fig. 1).

We provide evidence that the AF has declined over our study period. Our study also highlights again that uncertainties in LULCC emissions are large and need to be better constrained to fully understand the functioning of the global carbon cycle and aid future projections[34]. This would also benefit the assessment of the absolute sink strengths and is important for consistent country-level reporting of LULCC emissions, which will only become more important for monitoring progress towards mitigation goals.

Although the main result of our study stems from lower than previously reported LULCC emissions in the early part of our study period, it does affect carbon dynamics in the later period as well. For example, observed CO_2 concentrations in 2020 were roughly 2 ppm below those projected in the Representative Concentration Pathway 8.5 (RCP8.5) scenario (Extended Data Fig. 1, see Methods). This is often attributed to the levelling off of fossil fuel emissions after 2013 (ref. [35]). The difference between RCP8.5-projected and observed fossil fuel emissions is indeed increasing with time, but over the 2010–2019 period, this was partly compensated for by increased LULCC emissions[36] (Extended Data Fig. 2). Over the same period, the lower observed AF than the RCP8.5-projected AF (0.48 compared with 0.51) was another key reason for the lower-than-projected CO_2 concentration in 2020, contributing about 40% of the 2-ppm difference (Extended Data Fig. 1). This result, however, is very sensitive to the LULCC dataset used, which governs the degree to which declining fossil fuel emissions are offset by higher-than-expected LULCC emissions (Extended Data Fig. 3) and reiterates the need for better-constrained LULCC emissions.

Although our results shed new light on the functioning of the global carbon cycle over the past six decades, the declining trend cannot be extrapolated to the future. The AF is affected by the trajectory of fossil fuel emissions[7,37], and non-linearities in climate–carbon interactions[8] may reverse the trend. In fact, the declining trend is mostly apparent when the full study period is taken into account; over the past two to three decades, the AF was stable or even increasing (Fig. 3). Process-based studies are needed to reconcile these patterns and to

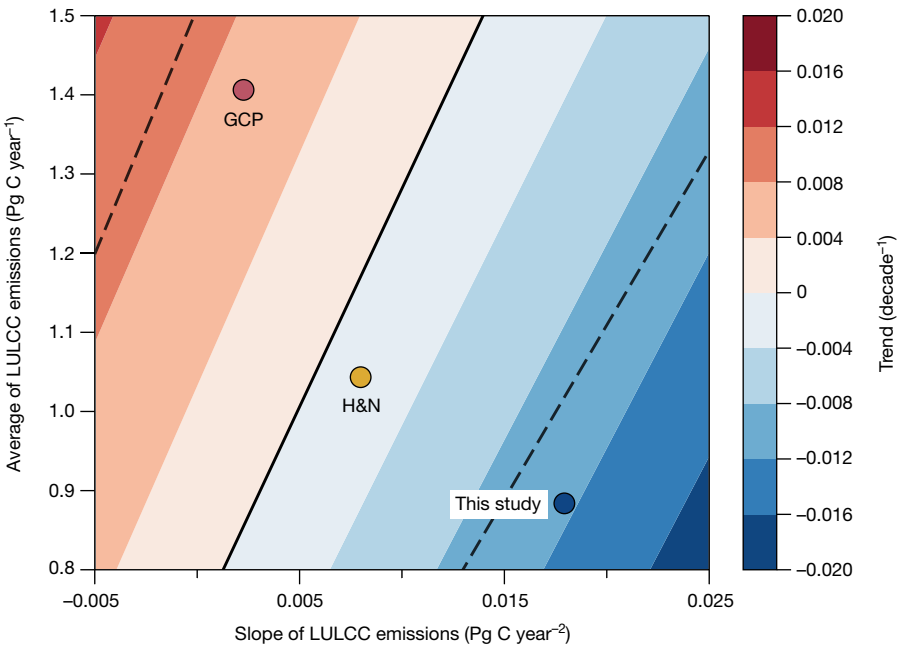

Fig. 4 | Sensitivity of the AF trend to average annual LULCC emissions and its slope. The labelled dots represent the AF trends for 1959–2019 using our LULCC emissions ('This study'), the GCP estimates based on Friedlingstein et al. (2020)[11] and estimates based on Houghton and Nassikas (2017)[27]. The time series were corrected for the effect of ENSO and volcanoes and subjected to bootstrapping, following the filter + bootstrap data treatment (see Methods). The solid black line is the zero AF trend line and the dashed lines show the standard deviation of the slope around zero. Slope mean and standard deviation were on the basis of a Monte Carlo simulation with n = 1,000 (see Methods).

also be in a better position to make informed predictions about future sink behaviour.

The underlying sink mechanisms have been widely explored and include enhanced oceanic carbon uptake related to increasing biological activity[38], increasing terrestrial carbon uptake owing to enhanced nutrient deposition[39], CO_2 fertilization[8], changes in diffuse radiation resulting in increasing canopy photosynthesis[40] and, more recently, reduced respiration during the warming hiatus[41]. Our results imply that these mechanisms as a whole may be more effective than previously thought. One line of evidence supporting this comes from revised interpretation of the ocean carbon sink, which may be substantially higher than often assumed[42], potentially offsetting a declining land sink strength[43]. However, it is crucial to recognize that the estimation of the combined sink strength by analysis of the AF cannot explain the underlying mechanisms that cause the increased efficiency. Nonetheless, our analysis using the most recent insights in LULCC variability over time implies that the carbon–climate system as a whole has been remarkably stable and may have even become more efficient when considering the full period of CO_2 measurements.

Online content

Any methods, additional references, Nature Research reporting summaries, source data, extended data, supplementary information, acknowledgements, peer review information; details of author contributions and competing interests; and statements of data and code availability are available at https://doi.org/10.1038/s41586-021-04376-4.

1. Canadell, J. G. et al. in *Climate Change 2021: The Physical Science Basis. Contribution of Working Group I to the Sixth Assessment Report of the Intergovernmental Panel on Climate Change* (eds Masson-Delmotte, V. et al.) (Cambridge Univ. Press, 2021) (in the press).
2. McKinley, G. A., Fay, A. R., Takahashi, T. & Metzl, N. Convergence of atmospheric and North Atlantic carbon dioxide trends on multidecadal timescales. *Nat. Geosci.* **4**, 606–610 (2011).
3. Schuur, E. A. G. et al. Climate change and the permafrost carbon feedback. *Nature* **520**, 171–179 (2015).
4. Le Quéré, C., Raupach, M. R., Canadell, J. G. & Al, G. M. Trends in the sources and sinks of carbon dioxide. *Nat. Geosci.* **2**, 831–836 (2009).
5. Raupach, M. R. et al. The declining uptake rate of atmospheric CO_2 by land and ocean sinks. *Biogeosciences* **11**, 3453–3475 (2014).
6. Knorr, W. Is the airborne fraction of anthropogenic CO_2 emissions increasing? *Geophys. Res. Lett.* **36**, L21710 (2009).
7. Gloor, M., Sarmiento, J. L. & Gruber, N. What can be learned about carbon cycle climate feedbacks from the CO_2 airborne fraction? *Atmos. Chem. Phys.* **10**, 7739–7751 (2010).
8. Keenan, T. F. et al. Recent pause in the growth rate of atmospheric CO_2 due to enhanced terrestrial carbon uptake. *Nat. Commun.* **7**, 13428 (2016).
9. Sarmiento, J. L. et al. Trends and regional distributions of land and ocean carbon sinks. *Biogeosciences* **7**, 2351–2367 (2010).
10. Ballantyne, A. P., Alden, C. B., Miller, J. B., Tans, P. P. & White, J. W. C. Increase in observed net carbon dioxide uptake by land and oceans during the past 50 years. *Nature* **488**, 70–72 (2012).
11. Friedlingstein, P. et al. Global carbon budget 2020. *Earth Syst. Sci. Data* **12**, 3269–3340 (2020).
12. Mahowald, N. M. et al. Interactions between land use change and carbon cycle feedbacks. *Global Biogeochem. Cycles* **31**, 96–113 (2017).
13. Field, R. D., van der Werf, G. R. & Shen, S. S. P. Human amplification of drought-induced biomass burning in Indonesia since 1960. *Nat. Geosci.* **2**, 185–188 (2009).
14. van Marle, M. J. E. et al. Fire and deforestation dynamics in Amazonia (1973–2014). *Global Biogeochem. Cycles* **31**, 24–38 (2017).
15. Morton, D. C. et al. Cropland expansion changes deforestation dynamics in the southern Brazilian Amazon. *Proc. Natl Acad. Sci. USA* **103**, 14637–14641 (2006).
16. van Wees, D. et al. The role of fire in global forest loss dynamics. *Glob. Change Biol.* **27**, 2377–2391 (2021).
17. Cox, P. M., Betts, R. A., Jones, C. D., Spall, S. A. & Totterdell, I. J. Acceleration of global warming due to carbon-cycle feedbacks in a coupled climate model. *Nature* **408**, 184–187 (2000).
18. Friedlingstein, P. & Prentice, I. Carbon–climate feedbacks: a review of model and observation based estimates. *Curr. Opin. Environ. Sustain.* **2**, 251–257 (2010).
19. Pan, Y. et al. A large and persistent carbon sink in the world's forests. *Science* **333**, 988–993 (2011).
20. Piao, S. et al. Net carbon dioxide losses of northern ecosystems in response to autumn warming. *Nature* **451**, 49–52 (2008).
21. Hubau, W. et al. Asynchronous carbon sink saturation in African and Amazonian tropical forests. *Nature* **579**, 80–87 (2020).
22. Le Quéré, C. et al. Saturation of the Southern Ocean CO_2 sink due to recent climate change. *Science* **316**, 1735–1738 (2007).
23. Miettinen, J., Shi, C. & Liew, S. C. Deforestation rates in insular Southeast Asia between 2000 and 2010. *Glob. Change Biol.* **17**, 2261–2270 (2011).
24. Morton, D. C. et al. Agricultural intensification increases deforestation fire activity in Amazonia. *Glob. Change Biol.* **14**, 2262–2275 (2008).
25. Otón, G., Lizundia-Loiola, J., Pettinari, M. L. & Chuvieco, E. Development of a consistent global long-term burned area product (1982–2018) based on AVHRR-LTDR data. *Int. J. Appl. Earth Obs. Geoinf.* **103**, 102473 (2021).
26. van der Werf, G. R. et al. Global fire emissions estimates during 1997–2016. *Earth Syst. Sci. Data* **9**, 697–720 (2017).
27. Houghton, R. A. & Nassikas, A. A. Global and regional fluxes of carbon from land use and land-cover change 1850–2015. *Global Biogeochem. Cycles* **31**, 456–472 (2017).
28. Brondizio, E. S. & Moran, E. F. Level-dependent deforestation trajectories in the Brazilian Amazon from 1970 to 2001. *Popul. Environ.* **34**, 69–85 (2012).
29. Houghton, R. A. How well do we know the flux of CO_2 from land-use change? *Tellus B Chem. Phys. Meteorol.* **62**, 337–351 (2010).
30. van der Werf, G. R. et al. Continental-scale partitioning of fire emissions during the 1997 to 2001 El Niño/La Niña period. *Science* **303**, 73–76 (2004).
31. Tans, P. & Keeling, R. Trends in atmospheric carbon dioxide. *National Oceanic & Atmospheric Administration, Earth System Research Laboratories (NOAA/ESRL) and Scripps Institution of Oceanography*. http://www.esrl.noaa.gov/gmd/ccgg/trends/ and http://scrippsco2.ucsd.edu/ (accessed 24 January 2021).
32. Boden, T. A., Marland, G. & Andres, R. J. Global, regional, and national fossil-fuel CO_2 emissions. *Carbon Dioxide Information Analysis Center, Oak Ridge National Laboratory, U.S. Department of Energy*. http://cdiac.ornl.gov/trends/emis/overview_2013.html https://doi.org/10.3334/CDIAC/00001_V2016 (2016).
33. Ramo, R. et al. African burned area and fire carbon emissions are strongly impacted by small fires undetected by coarse resolution satellite data. *Proc. Natl Acad. Sci. USA* **118**, e2011160118 (2021).
34. Booth, B. B. B. et al. Narrowing the range of future climate projections using historical observations of atmospheric CO_2. *J. Clim.* **30**, 3039-–3053 (2017).
35. Hausfather, Z. & Peters, G. P. Emissions – the 'business as usual' story is misleading. *Nature* **577**, 618–620 (2020).
36. Schwalm, C. R., Glendon, S. & Duffy, P. B. RCP8.5 tracks cumulative CO_2 emissions. *Proc. Natl Acad. Sci. USA* **117**, 19656–19657 (2020).
37. Jones, C. et al. Twenty-first-century compatible CO_2 emissions and airborne fraction simulated by CMIP5 earth system models under four representative concentration pathways. *J. Clim.* **26**, 4398–4413 (2013).
38. Gruber, N. Carbon at the coastal interface. *Nature* **517**, 148–149 (2015).
39. Zaehle, S. & Friend, A. D. Carbon and nitrogen cycle dynamics in the O-CN land surface model: 1. Model description, site-scale evaluation, and sensitivity to parameter estimates. *Global Biogeochem. Cycles* **24**, GB1005 (2010).
40. Mercado, L. M. et al. Impact of changes in diffuse radiation on the global land carbon sink. *Nature* **458**, 1014–1017 (2009).
41. Ballantyne, A. et al. Accelerating net terrestrial carbon uptake during the warming hiatus due to reduced respiration. *Nat. Clim. Change* **7**, 148–152 (2017).
42. Watson, A. J. et al. Revised estimates of ocean-atmosphere CO_2 flux are consistent with ocean carbon inventory. *Nat. Commun.* **11**, 4422 (2020).
43. Wang, S. et al. Recent global decline of CO_2 fertilization effects on vegetation photosynthesis. *Science* **370**, 1295–1300 (2020).
44. Trade. FAOSTAT online database. *Food and Agriculture Organization of the United Nations* http://www.fao.org/faostat/en/#data (accessed 19 August 2021).

Methods

Calculation of the airborne fraction

The CO_2 flux mass balance in the global atmosphere can be written as:

$$dA_{CO2}/dt = E_{FF} + E_{LU} - S_O - S_L \quad (1)$$

in which A_{CO2} is the atmospheric CO_2 concentration and its derivative, dA_{CO2}, is the atmospheric growth rate, E_{FF} is the fossil-fuel-emissions flux, E_{LU} is the LULCC emissions flux and S_O and S_L are the ocean and land sinks, respectively. In turn, the AF can be calculated as:

$$AF = \frac{E_{LU} + E_{FF} - S_O - S_L}{E_{LU} + E_{FF}} = \frac{dA_{CO2}/dt}{E_{LU} + E_{FF}} = 1 - SF \quad (2)$$

The AF is the fraction of anthropogenic CO_2 that accumulates in the atmosphere, dependent on the balance between anthropogenic emission fluxes and sink fluxes (sink fraction; SF). The AF and its trend were determined and compared for three different LULCC emission scenarios: GCP, H&N and our estimates (referred to as 'this study'). For all three scenarios, the datasets used for atmospheric CO_2 concentrations and fossil fuel emissions were kept the same and on the basis of the data sources described below. We first describe the datasets, followed by a description of uncertainties and trend sensitivity.

Atmospheric CO_2 concentrations

Atmospheric CO_2 concentrations were on the basis of mean monthly observations taken under the Scripps CO_2 programme at MLO (in situ and flasks) and SPO (flask measurements) for 1958–2019 (ref. [31]). This dataset was adjusted by removal of the quasi-regular seasonal cycle and missing values were filled using a smooth fit. Our atmospheric CO_2 time series is composed as the average over the MLO and SPO concentrations. Concentrations of CO_2 in ppm were converted to Pg C by multiplication with a conversion factor of 2.134.

Fossil fuel combustion and cement production

We used fossil fuel emission estimates (E_{FF}) from the GCP, which were based on national energy statistics[45]. Although uncertainty in E_{FF} is, in general, lower than E_{LU} (see below) and is taken into account in our trend analyses, we tested the sensitivity of our results by replacing E_{FF} in China as reported in the GCP with an alternative study based on revised energy statistics and more representative emission factors[46]. In that study, E_{FF} from China for 1959–2013 were lower than in the GCP. We extended the data beyond 2013 on the basis of GCP E_{FF} values for China over 2013–2019 and the relative difference between Liu et al. (2015)[46] and the GCP for the overlapping 2010–2013 period. Given that E_{FF} from China grew more rapidly than global E_{FF} over our study period, lower E_{FF} from China could offset part of the increase in E_{LU}. This observation could lead to a higher AF towards the end of our study period, with a more positive AF trend as a result. However, using these lower E_{FF} for China instead of the GCP values did not appreciably change the robustness of found trends (Fig. 3f, 'Lower FF emissions China').

LULCC data based on Houghton and Nassikas

The revised bookkeeping model is a seamless historical country-level dataset of LULCC emissions from the period 1850–2015, which we extended for 2016–2019 on the basis of the 2011–2015 average emissions, as other datasets showed relatively little change during this period[11]. This model uses country-based statistics of rates of deforestation and reforestation from FRA 2015 (Global Forest Resources Assessment) and annual changes in croplands and pastures from the Food and Agriculture Organization Statistics Division (FAOSTAT)[47]. Furthermore, the H&N dataset also considers carbon emissions from the draining and burning of peatlands in Southeast Asia[48]. The bookkeeping model accounts for carbon initially held in areas affected by LULCC and subsequently tracks changes in four pools (living aboveground and belowground biomass; dead biomass, including coarse woody debris; harvested wood products; and soil organic carbon). The amount of CO_2 emitted into the atmosphere is based on emissions released during deforestation, logging and degradation, as well as conversion of forest into agricultural or degraded land owing to logging, forest fires, or soil and vegetation decay. The bookkeeping model tracks how much carbon is sequestered from the atmosphere and thereafter stored in biomass and soil, also during regrowth and soil build-up after land use change. It considers transitions between forests, pastures and cropland; shifting cultivation; degradation of forests where a fraction of the trees is removed; abandonment of agricultural land; and forest management, such as wood harvest and, in the USA, fire management.

LULCC data from the Global Carbon Project

Within the GCP (www.globalcarbonproject.org), emissions related to LULCC (E_{LU}) include carbon fluxes from deforestation, afforestation, logging and forest degradation (including harvest activity), shifting cultivation and regrowth of forests following wood harvest or abandonment of agriculture[11]. These emissions are quantified on the basis of three bookkeeping approaches; the bookkeeping of land use emissions model (BLUE)[49], Houghton and Nassikas (2017)[27] and the estimate published by Gasser et al. (2020)[50] using the compact Earth system model OSCAR. The number used in the GCP is the average of the three models. Although all three models are based on the bookkeeping approach of Houghton (2003)[47], they differ with respect to the land-use-change data used, spatial resolution and a myriad of other factors[11].

Visibility-based fire emissions

Fire-emitted aerosols lower visibility, enabling visibility observations to be used as a proxy for fire emissions[13,14]. We used visibility-based fire emissions for the two largest deforestation regions; EQAS and the ARCD in South America. Observations for these regions started in 1960 and 1973, respectively (Extended Data Fig. 4). Visibility data originate from weather station records from the NOAA National Centers for Environmental Information (NCEI) Integrated Surface Database (ISD). Visibility was transformed into an extinction coefficient (B_{ext}), which shows sharp increases during sustained periods of fire emissions. The visibility observations showed a close link between fire emissions and population dynamics, droughts and deforestation[13,14]. In Indonesia, the link between visibility and fire is very good: total particulate matter estimates from the Global Fire Emissions Database (GFED) correspond with B_{ext} for both Sumatra ($R^2 = 0.91$) and Kalimantan ($R^2 = 0.85$) for the 1997–2006 period[13] and there is also good agreement in subsequent years[51]. The correlation between B_{ext} and fire in the ARCD is reasonable to good. On a local scale with one station, this resulted in an R^2 of 0.84 between monthly B_{ext} observations and surface measurements of PM_{10} (ref. [14]). On a more regional scale, the R^2 between both datasets was 0.61 during the dry season only (covering 95–98% of all emissions in that region).

From fire emissions to LULCC emissions

The visibility observations were converted to a time series of fire emissions using satellite-based estimates of the GFED version 4s (GFED4s) for the overlapping 1997–2015 period[26]. In the ARCD, no visibility observations were available between 1959 and 1973. Emissions for this period were kept constant at the lowest decadal average. This dataset was published as the historic global biomass burning emissions for the CMIP6 (BB4CMIP) database[52], consisting of visibility-based emissions before 1997 and GFED4s emissions since 1997.

In this study, these fire emissions were used to develop estimates of E_{LU} ('this study'). Emissions for the ARCD were supplemented with a decomposition component on the basis of the average annual fire emissions over that year and the nine preceding years, assuming an equal contribution of fire and other loss pathways to total emissions[53].

A similar approach was used for EQAS but only for non-peat fire emissions. These emissions were supplemented with emissions coming from oxidation related to peat drainage[48]. Extended Data Figure 4 provides an overview of the input data used, what time periods they are available for and how they were combined to reconstruct E_{LU} ('this study').

To account for uncertainty in the ratio between emissions by means of fire versus decomposition and other pathways, we included a scenario in which the fire contribution increased in a linear fashion from 25 to 50% over our study period. This boosts emissions early in our study period, making the AF trend more positive. However, this scenario did not cause a substantial change in trend estimates (Fig. 3f, 'Increasing role of fire').

Uncertainties in the datasets

For dA_{CO2}, we used the globally determined standard error from Dlugokencky and Tans (2021)[54], which translates to a 1σ uncertainty of roughly 0.6 Pg C year^{-1} in the first two decades until 1979 and an uncertainty of about 0.2 Pg C year^{-1} from then onwards. For E_{FF}, the uncertainty was estimated at σ = 5% (ref. [32]). However, biases in the emissions of China could lead to higher uncertainties than reported[46,55]. Therefore, the E_{FF} uncertainties for China were on the basis of found biases[46], with a minimum uncertainty of σ = 10% (ref. [55]). In addition, we performed a sensitivity analysis with lower emissions for China, in which we took the data source with the largest difference with the GCP to assess the robustness of our trend (see section 'Emissions from fossil fuel combustion and cement production'). Uncertainties in E_{LU} emissions are often poorly characterized. Houghton and Nassikas (2017)[27] reported a σ of 10.4%, whereas this is 50% in the GFED[26]. We assumed that the satellite-derived GFED estimates are more accurate than estimates partly based on country-level statistics and adopted a 50% uncertainty for the whole time period. On annual scales, uncertainties could be higher but the most relevant characteristic for our study is the long-term temporal evolution (Fig. 1), which we consider to be less uncertain, as it is rooted in a uniform approach. Uncertainties reported in the GCP E_{LU} are 0.7 Pg C year^{-1}, which corresponds to a relative uncertainty of about 40–60% over the study period[27]. For consistency, we have therefore adopted an uncertainty of 50% for all E_{LU} data. Uncertainties in AF in terms of 1σ were calculated by propagation of the reported standard errors through equation (2) using Monte Carlo simulation (see section below).

Estimation of trends in AF and trend uncertainty

Trends in AF were estimated on the basis of the annual time series over the full time period of available data (1959–2019). Trends were determined using the non-parametric Mann–Kendall test and Sen's slope estimator for the robustness of trends. Trends and trend uncertainty ranges were calculated as the median and standard deviation, respectively, of the trend results from a Monte Carlo simulation (n = 10,000). The simulation used normally distributed input errors on the basis of the 1σ uncertainty ranges of the various emission datasets (dA_{CO2}, E_{FF}, E_{LU}).

Monte Carlo simulations were performed for several data treatments, to test for AF trend robustness, largely following Raupach et al. (2014)[5]. These data treatments were: the raw AF time series ('raw'), smoothing and filtering of the atmospheric CO_2 monthly time series to reduce within-year variability and the influence of the ENSO and volcanic activity ('filter'), bootstrapping to test robustness dependency on the time series start and end points ('bootstrap') and combined filtering and bootstrapping ('filter + bootstrap'). For the filtered data treatment, the monthly atmospheric CO_2 flux time series was first smoothed using a 15-month moving average filter to reduce variability within years[5,56]. Next, interannual variability related to the ENSO and volcanic activity was reduced by subtraction of the part of the atmospheric CO_2 flux signal that was correlated to a combined ENSO–volcanic variability index (EVI). The ENSO index (ENSO) was based on anomalies in Niño3 sea surface temperatures (SSTs), with a lag of four months between concentrations and SSTs (SSTs leading). This index was combined with the volcanic aerosol index (VAI)[57] into the EVI. The relative contribution of the VAI in relation to the ENSO was determined by maximizing the correlation between:

$$\mathrm{EVI}(t) = \mathrm{ENSO}(t-\tau) + \lambda \mathrm{VAI}(t) \quad (3)$$

and the CO_2 growth rate. Here λ is the relative weight of the VAI compared with the ENSO, for which we found a value of −17.3. For convenience and to remain consistent with Raupach et al. (2008)[56], a value of λ = −16 was used. The EVI noise removal was performed by minimization of the variance in:

$$U(t) = (\mathrm{d}A_{CO2})/\mathrm{d}t - \mu \mathrm{EVI}(t) \quad (4)$$

in which U is the noise-reduced atmospheric growth rate (the uncorrelated part), τ is the four-month time lag and μ is the sensitivity factor, with values around 0.9 and 0.6 for time series with or without a 15-month moving average, respectively.

For the bootstrapping data treatment, a continuous segment of the AF time series with random length and start and end points was picked with replacement, carried out for each Monte Carlo iteration. The minimum segment length was constrained to be at least a fraction f_{Bts} = 0.8, following Raupach et al. (2014)[5].

Sensitivity of the AF trends

As a further investigation of the sensitivity of trends in AF to the E_{LU} dataset used, we calculated the trend in AF for a range of linear E_{LU} time series with different combinations of average value and slope (Fig. 4). We varied the 1959–2019 average of the linear approximation of E_{LU} from 0.8 to 1.5 Pg C year^{-1} and the slope from −0.005 to 0.025 Pg C year^{-2}, encompassing the range of average and slope values covered by the three E_{LU} datasets studied. A Monte Carlo simulation (with n = 1,000) was used for each of the slope-averaged combinations in a 51 × 51 grid, to calculate trend sensitivity to E_{LU}. This Monte Carlo simulation was identical to the one previously described, with the 'filter + bootstrap' data treatment applied. AF trend estimates on the basis of the actual E_{LU} time series as compared with their linear approximations showed a maximum difference in trend estimate of 3% for the filtered data treatment and 26% for the filter + bootstrap data treatment. This shows that the use of a linear approximation of E_{LU} gives a relatively robust first-order indication of the AF trend.

Comparison against RCP8.5

We compared the observed evolution of A_{CO2}, E_{FF} and E_{LU} with that of the highest RCP scenario as used in the Intergovernmental Panel on Climate Change (IPCC) Fifth and Sixth Assessment Reports (AR5 and AR6), the RCP8.5 scenario[58]. This was done for cumulative E_{FF} and E_{LU} for 2010–2019 bounded by A_{CO2} for 2010 and 2020 to have 10 years of emissions and a 10-year atmospheric evolution period. Sink strength was calculated as the residual. To make for a fair comparison, A_{CO2} for 2010 from RCP8.5 was aligned with observed values for 2010. Given that this time period was almost ENSO neutral as a whole and that the observed AF mimicked ENSO-corrected values within 0.2%, we have used the raw observations for Extended Data Figs. 1 and 3.

Data availability

GCP data are publicly available at https://www.globalcarbonproject.org/carbonbudget. The ENSO index was based on anomalies in Niño 3 SSTs, which are publicly available at https://psl.noaa.gov/gcos_wgsp/Timeseries/Data/nino3.long.anom.data. Gridded visibility-based fire emissions can be found at the CMIP6 forcing data repository (https://esgf-node.llnl.gov/search/input4mips/). All input data, including the Houghton and Nassikas dataset[27], have been made available at https://doi.org/10.5281/zenodo.5617953.

Code availability

The Python code that was used to assimilate the raw data and perform the analyses is available at https://doi.org/10.5281/zenodo.5617953.

45. Gilfillan, D. & Marland, G. CDIAC-FF: global and national CO_2 emissions from fossil fuel combustion and cement manufacture: 1751–2017. *Earth Syst. Sci. Data* **13**, 1667–1680 (2021).
46. Liu, Z. et al. Reduced carbon emission estimates from fossil fuel combustion and cement production in China. *Nature* **524**, 335–338 (2015).
47. Houghton, R. A. Revised estimates of the annual net flux of carbon to the atmosphere from changes in land use and land management 1850–2000. *Tellus B Chem. Phys. Meteorol.* **55**, 378–390 (2003).
48. Hooijer, A. et al. Current and future CO_2 emissions from drained peatlands in Southeast Asia. *Biogeosciences* **7**, 1505–1514 (2010).
49. Hansis, E., Davis, S. J. & Pongratz, J. Relevance of methodological choices for accounting of land use change carbon fluxes. *Global Biogeochem. Cycles* **29**, 1230–1246 (2015).
50. Gasser, T. et al. Historical CO_2 emissions from land use and land cover change and their uncertainty. *Biogeosciences* **17**, 4075–4101 (2020).
51. Field, R. D. et al. Indonesian fire activity and smoke pollution in 2015 show persistent nonlinear sensitivity to El Niño-induced drought. *Proc. Natl Acad. Sci. USA* **113**, 9204–9209 (2016).
52. van Marle, M. J. E. et al. Historic global biomass burning emissions for CMIP6 (BB4CMIP) based on merging satellite observations with proxies and fire models (1750–2015). *Geosci. Model Dev.* **10**, 3329–3357 (2017).
53. van der Werf, G. R. et al. CO_2 emissions from forest loss. *Nat. Geosci.* **2**, 737–738 (2009).
54. Dlugokencky, E. & Tans, P. Trends in atmospheric carbon dioxide. *National Oceanic & Atmospheric Administration, Earth System Research Laboratory (NOAA/ESRL)* http://www.esrl.noaa.gov/gmd/ccgg/trends/gl_gr.html (accessed 19 August 2021).
55. Gregg, J. S., Andres, R. J. & Marland, G. China: emissions pattern of the world leader in CO_2 emissions from fossil fuel consumption and cement production. *Geophys. Res. Lett.* **35**, L08806 (2008).
56. Raupach, M. R., Canadell, J. G. & Le Quéré, C. Anthropogenic and biophysical contributions to increasing atmospheric CO_2 growth rate and airborne fraction. *Biogeosciences* **5**, 1601–1613 (2008).
57. Ammann, C. M. A monthly and latitudinally varying volcanic forcing dataset in simulations of 20th century climate. *Geophys. Res. Lett.* **30**, 483–487 (2003).
58. Riahi, K. et al. RCP 8.5—a scenario of comparatively high greenhouse gas emissions. *Clim. Change* **109**, 33–57 (2011).

Acknowledgements This research was funded by the European Research Council (ERC) grant number 280061 and the Netherlands Organization for Scientific Research (NWO) (Vici scheme research programme, no. 016.160.324).

Author contributions G.R.vdW. designed the research, M.J.E.vM., R.D.F. and R.A.H. constructed the LULCC time series, D.vW. performed the AF trend analysis with help from J.V., the paper was written by D.vW., M.J.E.vM. and G.R.vdW.

Competing interests The authors declare no competing interests.

Additional information

Correspondence and requests for materials should be addressed to Guido. R. van der Werf.

Peer review information *Nature* thanks Emilio Chuvieco, Chris Jones and Tom Oda for their contribution to the peer review of this work.

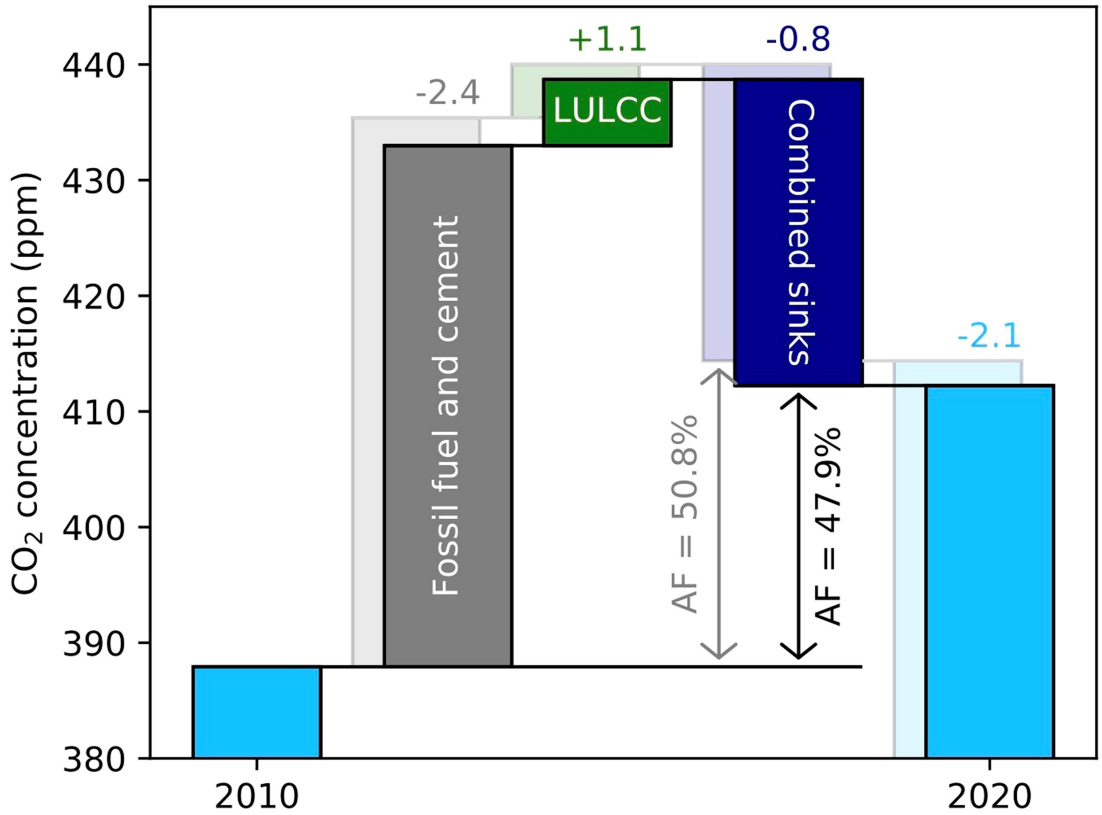

Extended Data Fig. 1 | RCP8.5-projected and observed evolution of atmospheric CO_2 growth using our LULCC data. RCP8.5-projected (background) and observed (forefront) atmospheric CO_2 growth over 2010–2020 on the basis of observed concentrations, sources from fossil fuel burning, cement manufacturing and LULCC based on this study. Sink strength is computed as the residual. AF is short for airborne fraction and the numbers indicate what the difference is between observed values and RCP8.5 projections for each component.

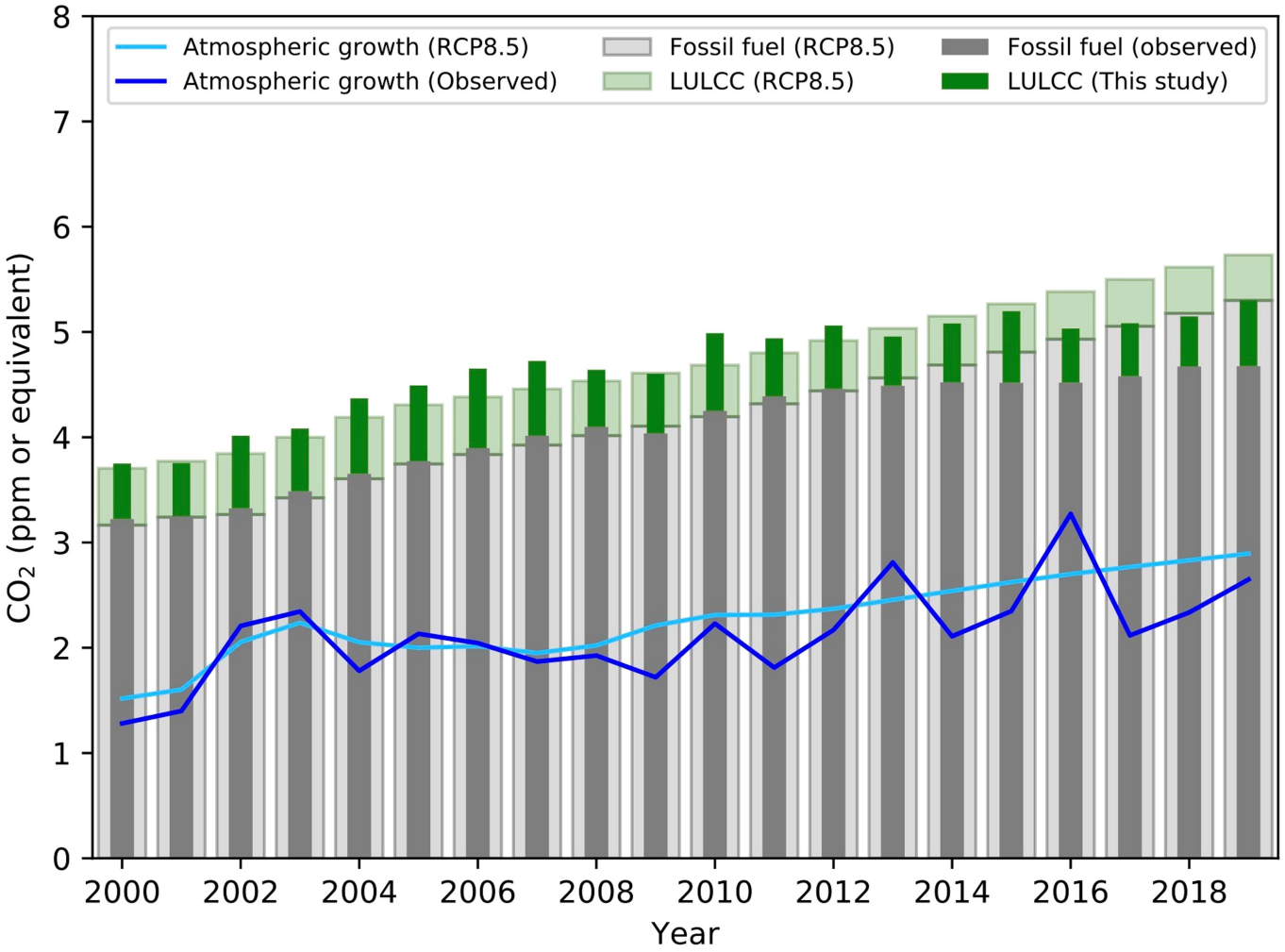

Extended Data Fig. 2 | Evolution of RCP8.5-projected and observed anthropogenic emissions and atmospheric CO_2 growth rate over 2000–2019. Fossil fuel emissions increased less than projected in RCP8.5 after 2012, but this was partly compensated for by higher-than-projected LULCC emissions in most years.

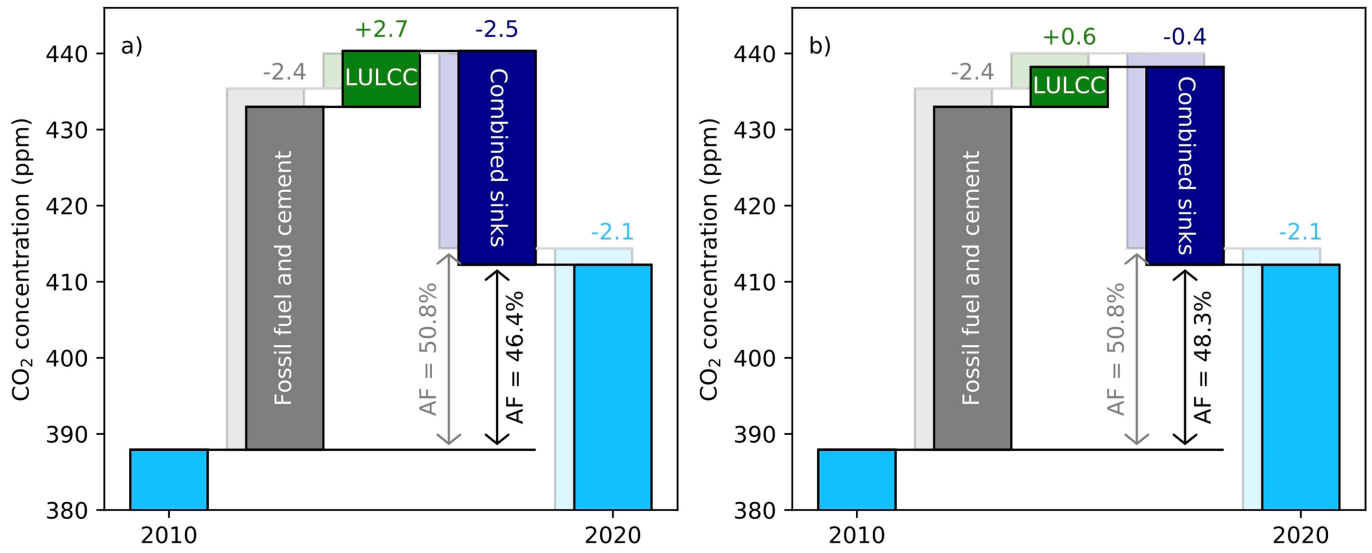

Extended Data Fig. 3 | RCP8.5-projected and observed evolution of atmospheric CO_2 growth on the basis of other LULCC datasets. RCP8.5-projected (background) and observed (forefront) evolution of atmospheric CO2 growth over 2010–2020 on the basis of observed concentrations, sources from fossil fuel burning, cement manufacturing and LULCC on the basis of the GCP (**a**) and H&N (**b**). Sink strength is computed as the residual. AF is short for airborne fraction and the numbers indicate what the difference is between observed values and RCP8.5 projections for each component.

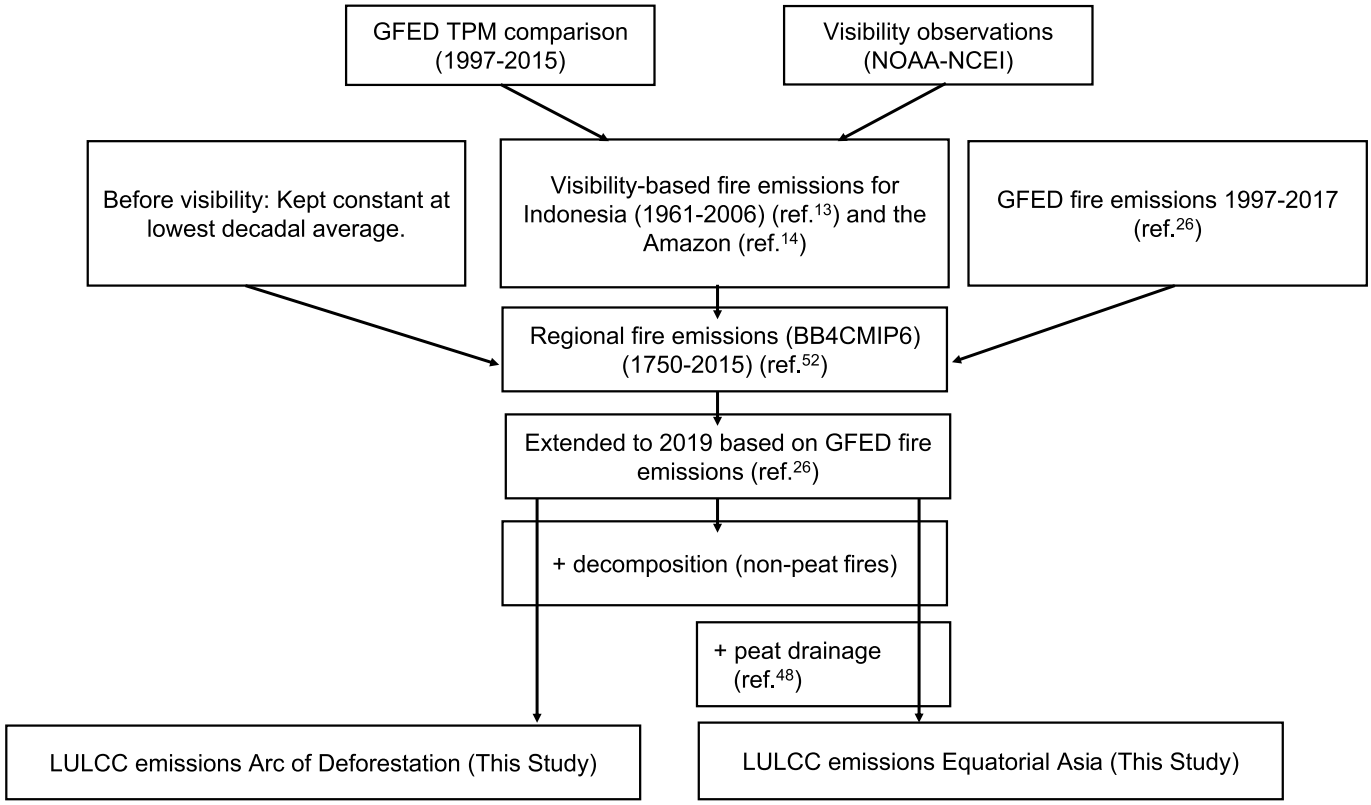

Extended Data Fig. 4 | Schematic overview for production of LULCC emissions. This overview shows our method to construct LULCC emissions on the basis of fire emissions in key deforestation zones of GFED4s (1997–2019) and visibility-based B_{ext} anchored to GFED4s for the preceding period. These were supplemented by non-fire emissions including those stemming from peat dynamics in EQAS.